Rotor Design Options for Improving V-22 Whirl-Mode Stability

C. W. Acree, Jr.
Aerospace Engineer
NASA Ames Research Center, Moffett Field, CA
wacree@mail.arc.nasa.gov

ABSTRACT

A CAMRAD II model of the V-22 Osprey tiltrotor was constructed for the purpose of analyzing high-speed aeroelastic instabilities (whirl flutter). The effects of different modeling options were examined, including single and dual load-path models of the blade root, swashplate coupling to the hub or transmission, compressible and incompressible rotor aerodynamics, and drive-train models with and without internal flexibility. Different amounts of blade sweep outboard of $0.8R$ were modeled with the intent of improving whirl-mode damping. Tip mass offsets were also examined. Appropriate combinations of blade sweep and tip mass offset greatly improved whirl-mode damping.

NOTATION

Symbols:

C_{l_α}	lift-curve slope
M	Mach number
r_s	radial station for start of sweep
R	rotor radius
x_m	tip mass offset, positive forward
δ_3	kinematic pitch-flap coupling ratio
Λ	sweep angle, positive aft
Ω	rotor shaft speed

Abbreviations:

DLP	dual load path
SLP	single load path
AWB	antisymmetric wing beamwise bending
AWC	antisymmetric wing chordwise bending
AWT	antisymmetric wing torsion
APY	antisymmetric pylon yaw
ABT	afterbody torsion
SWB	symmetric wing beamwise bending
SWC	symmetric wing chordwise bending
SWT	symmetric wing torsion
SPY	symmetric pylon yaw

Presented at the American Helicopter Society 58th Annual Forum, Montréal, Quebec, Canada, June 11-13, 2002.

INTRODUCTION

With current tiltrotor technology, very stiff, thick wings of limited aspect ratio are essential to meet aeroelastic stability requirements. Such wings severely limit cruise efficiency and maximum speed. Larger and more efficient tiltrotors will need longer and lighter wings, for which whirl-mode flutter is a serious design issue. Whirl flutter is also a potential design challenge for unconventional configurations such as quad tiltrotors (Ref. 1). Numerous approaches to improving the whirl-mode airspeed boundary have been investigated, typically focusing on wing design (Ref. 2), active stability augmentation (Ref. 3), and variable geometry rotors (Ref. 4). The research reported here applies the much simpler approaches of sweeping the outboard blade sections and moving the balance weights at the tip well ahead of the elastic axis.

The idea of using sweep or offset masses to improve whirl-flutter margins is not new. The present research grew out of earlier efforts at NASA Ames Research Center (Ref. 5). Research along similar lines has been carried out elsewhere (Ref. 6), but for a different rotor and with different analytical methods. (Reference 7 analyzed the effects of sweep on proprotor performance, but whirl-mode stability was not the primary objective.)

Previous efforts at Ames focussed on the XV-15 rotor (Ref. 8). This is the first application of these design principles to a full V-22 rotor model in CAMRAD II. A previous publication (Ref. 9) presented results for a preliminary analytical model; significant improvements have since been made and are reported herein.

The new analysis includes a dual load-path blade model, a compressible-flow aerodynamic model, a representation of swashplate/rotor modal coupling, a drive-train model, and other new features. The relative importance of these modeling features for prediction of whirl flutter is discussed. The paper concludes with discussions of the effects of blade sweep and tip mass offsets on whirl-flutter margins.

The primary purpose of the model is to investigate the effects of design modifications to the rotor on whirl flutter. Accordingly, only minor effort has been given to performance or loads predictions, and no attention was paid to handling qualities or noise predictions. These issues should obviously be addressed in future research.

Reference 10 includes details of the V-22 CAMRAD II model, including complete listings of the program inputs and aerodynamic tables.

ROTOR MODEL

The V-22 tiltrotor was modeled with CAMRAD II Release 4.0 (Ref. 11). The rotor model is shown in Fig. 1. Rotor airfoils are shown merely to better reveal the blade twist, and do not capture the details of the inboard fairings; CAMRAD II derives its aerodynamic data from external look-up tables (C81 format).

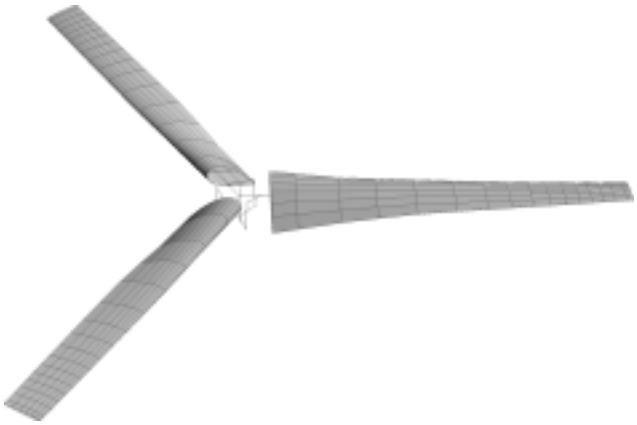

Fig. 1. CAMRAD II model of the V-22 rotor.

The V-22 rotor is stiff in-plane with a gimbaled hub and –15 deg pitch-flap coupling (δ_3). The structure is mostly composite, with a coning flexure and blade-fold hinges. The aerodynamic sections start with a 36-in (91-cm) chord at 5% radius, linearly tapering to a 22-in (56-cm) chord at the tip. The taper is interrupted by a bump over the blade-fold hinge. Total effective blade twist is 47.5 deg over a 228.5-in (5.80-m) radius. The quarter-chord locus is swept about 1 deg aft, with the quarter-chord line intersecting the pitch axis at 75% radius.

The V-22 CAMRAD II model is based on four sets of data:

1. Rotor structural data provided by Bell Helicopter Textron (Ref. 12), originally developed for Bell Helicopter's Myklestad program.
2. Rotor aerodynamic data, in the form of C81 tables, also provided by Bell Helicopter. The C81 tables are based on wind-tunnel test data of the rotor airfoils (Ref. 13).
3. Airframe geometry, converted from an earlier CAMRAD/JA model developed by Boeing Helicopters.
4. Airframe modal data, generated by MSC/NASTRAN SuperElement models of the V-22, provided by Bell Helicopter (Ref. 12; see also Ref. 14).

Additional data (unpublished) were provided by David A. Popelka and Jim C. Narramore of Bell Helicopter. The complete CAMRAD II model listings are given in Ref. 10. The rotor modeled is the Engineering and Manufacturing Development version.

Several variations of the model were also developed to better reveal the effects of different modeling options and input data, as discussed in the next section of this paper.

To calculate aeroelastic stability, CAMRAD II couples externally generated wing/pylon modes to an internally generated dynamic rotor model (Ref. 11). The wing/pylon modes were generated by a three-dimensional NASTRAN shell model (about 68,000 elements), with frequency adjustments based on flight- and ground-test data (Ref. 12). The structural damping of each mode was adjusted in accordance with test data, then increased by a constant value to approximate the effects of aerodynamic damping as given in Ref. 12.

The drive-train model included the engine and gearbox rotational inertias, drive-shaft and cross-shaft flexibilities, but no governor.

Aeroelastic Stability Analysis of Proprotors (ASAP) — the stability analysis used by Bell Helicopter and validated against flight-test data (Ref. 15) — was used to validate the CAMRAD II model of the unmodified V-22. Blade frequencies were validated against Bell Helicopter's Myklestad analysis (Ref. 15; see also Ref. 1), which generates inputs for ASAP. The whirl-flutter predictions were then checked against the ASAP predictions in Ref. 12.

Both ASAP and CAMRAD II were trimmed to zero power (windmill state), but with a drive train model. The V-22 has a flapping controller that minimizes flapping in flight; this was modeled in CAMRAD II simply by assuming axisymmetric, axial flow and by trimming to zero power with collective. This automatically yielded zero flapping. A further simplification was to trim only the rotor; given the

assumptions of axisymmetric flow and zero power, there was little to be gained by explicitly trimming the airframe. Accordingly, the automatic flight control system was not modeled. The rotor was trimmed to 332 rpm at 7500 ft (2300 m) altitude to match the ASAP predictions in Ref. 12.

Baseline Stability Predictions

Figures 2-5 show the whirl-flutter predictions for the complete CAMRAD II model. Frequency and damping are plotted against airspeed for symmetric and antisymmetric modes. These predictions are for level flight at zero power. Tracking the modes is problematic at high speeds because of the strong modal couplings, including multiple frequency crossings (Fig. 3), especially for the antisymmetric modes. Fortunately, the ambiguities are limited to high-frequency modes that do not determine the flutter boundary, so no significant effort was made to track and label all modal couplings.

For trim, blade deflections are calculated using nine flexible degrees of freedom per element (the CAMRAD II default; see Ref. 11). Flutter calculations included a gimbal for each rotor, eight dynamic and 16 quasi-static modes per blade, nine airframe modes, and seven drive-train modes. The dynamic blade modes were simply the eight lowest frequencies (up to 70 Hz, or 12/rev uncoupled); the quasi-static modes were arbitrarily set to twice the number of dynamic modes (further increases made negligible difference to the stability predictions). The airframe modes included wing beamwise and chordwise bending, wing torsion, and pylon yaw, separated into symmetric and antisymmetric modes, and the afterbody torsion mode; the airframe mode frequencies ranged from 2.9 to 8.6 Hz. The drive-train included rigid (azimuth) and flexible rotor, engine, and interconnect shaft modes.

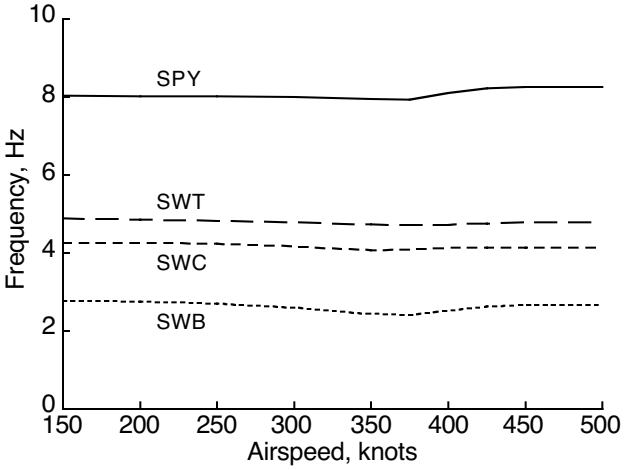

Fig. 2. Predicted frequencies of the V-22 symmetric wing/pylon modes.

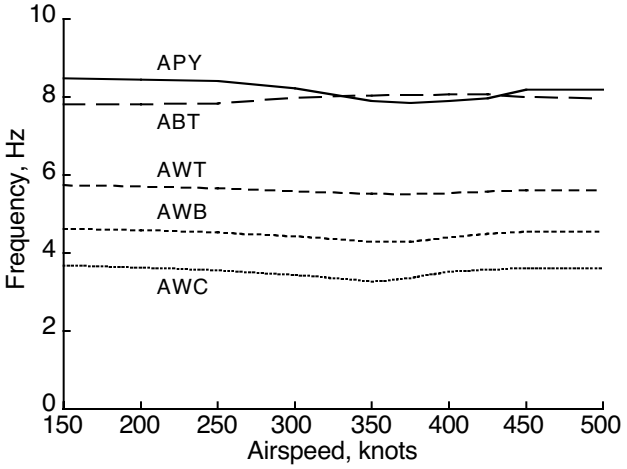

Fig. 3. Predicted frequencies of the V-22 antisymmetric wing/pylon modes.

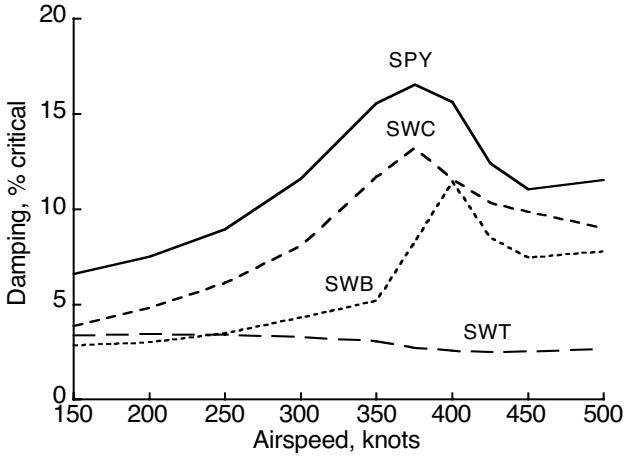

Fig. 4. Predicted damping of the V-22 symmetric wing/pylon modes.

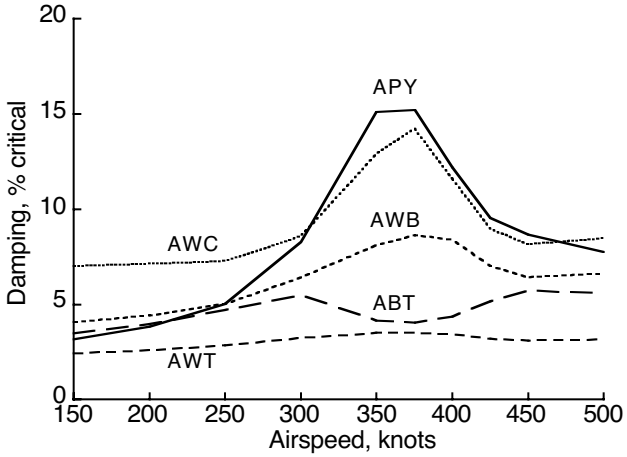

Fig. 5. Predicted damping of the V-22 antisymmetric wing/pylon modes.

Whirl-flutter predictions were also generated for trim with unlimited power (Ref. 10). With one exception, the results show higher damping up to at least 300 knots. A few modes, especially symmetric wing beamwise bending (SWB), have lower damping at higher speeds, but the power required for such speeds is physically unattainable, hence the reduction in damping is irrelevant in practice. The one exception is the afterbody torsion (ABT) mode, but it varies little with airspeed for both trim options and is not a critical mode. Because zero-power trim has the lowest damping for critical modes within the design flight envelope, it is appropriate for this study and was used for all predictions shown herein.

Effects of Modeling Options

Several different modeling options are compared in the following sections: dual load-path (DLP) and single load-path (SLP) models, rigid and flexible swashplate models, three different drive train models, and several different aerodynamic models.

Single load path versus dual load path

The V-22 hub comprises three composite arms, or yokes, connected to the shaft by a constant-velocity joint. The yokes gimbal as a unit, but do not pitch with the blades. Centrifugal loads and flap and lag moments are carried by the yokes. Pitching moments, hence control loads, for each blade are carried by a hollow pitch case ("grip") that surrounds the yoke and pitches with the blade. The blades are attached to the outer ends of the grips. Figure 6 shows the V-22 yoke and grip; Fig. 7 schematically illustrates the key structural elements. (Figure 6 is based on information in Ref. 12; see also Ref. 16.)

Each yoke is much less stiff in flap than in lag, such that it constitutes a coning flexure; the at-rest precone is 2.75 deg. The large lag stiffness places the first lag frequency above 1/rev for all flight conditions, so that the rotor is by definition stiff in-plane.

The grip is connected to the yoke by a series of elastomeric bearings that allow the large changes in pitch needed between hover and high-speed flight. Two pitch-change bearings at (approximately) the inboard and outboard ends of the yoke accommodate blade pitch and transmit shear loads from the grip to the yoke. A separate bearing transmits centrifugal loads. The elastomeric bearings allow a small amount of in-plane and out-of-plane cocking of the grip with respect to the yoke, in order to accommodate flexing of the yoke as the coning angle changes.

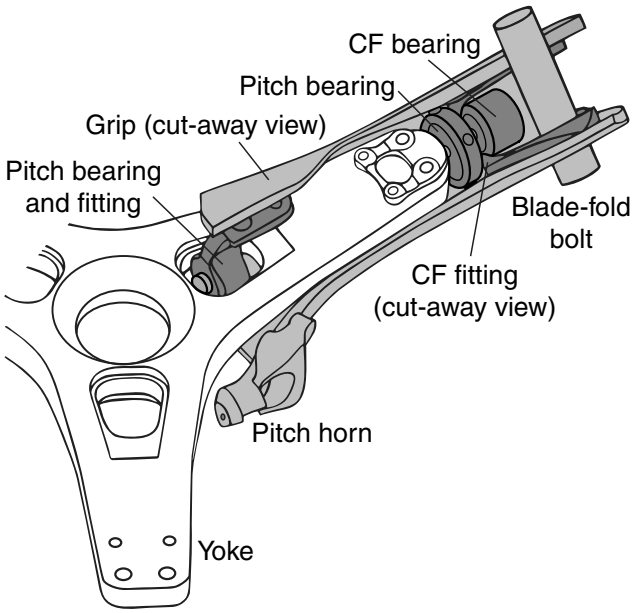

Fig. 6. V-22 yoke and grip; pitching components are shaded.

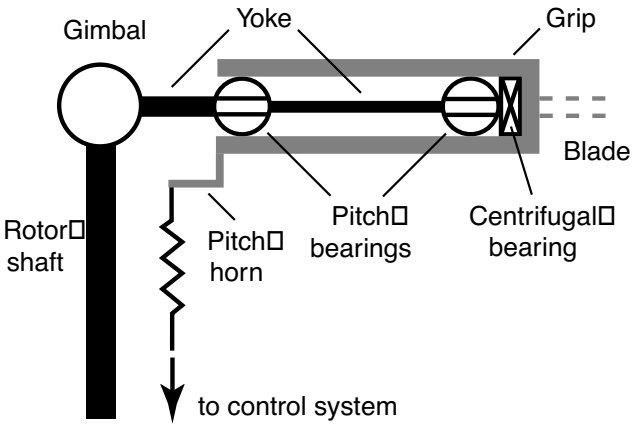

Fig. 7. Schematic of grip and yoke assembly.

Figures 8 and 9 illustrate the single load-path and dual load-path variants. For the first, the grip and blade are assumed to pivot about the inboard bearing for coning, flap, and lag motions, with the yoke flexibility modeled as flap and lag springs (only the flap spring is shown in the figure). The pitch bearing is modeled separately and placed slightly outboard of the flap/lag bearing, in order to prevent the flap and lag springs from rotating with pitch. The SLP model of Fig. 8 is conceptually similar to the original V-22 rotor design, which did not have a coning flexure (Ref. 17).

For the dual load-path variant (Fig. 9), the yoke and grip are modeled as separate load paths, and the bearings are modeled with transverse flexibility (two axes) and rotational flexibility (three axes). Only the grip rotates freely in pitch. The centrifugal bearing is assumed to be coincident with the outer pitch bearing. The inboard pitch bearing is axially free, but the outboard bearing is axially rigid, so that all centrifugal loads are taken by the outboard bearing.

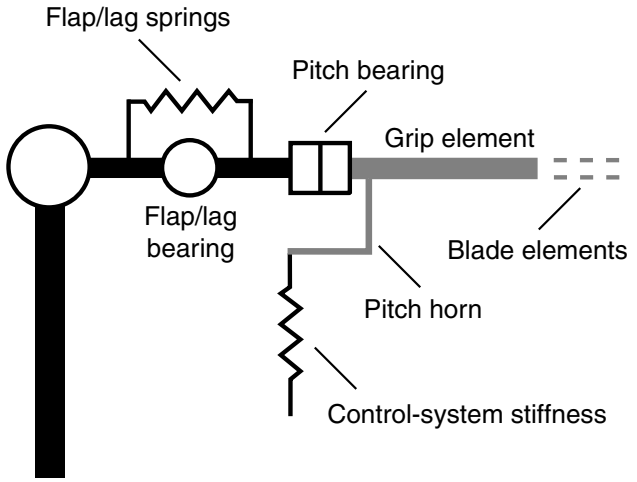

Fig. 8. Schematic of single load-path model.

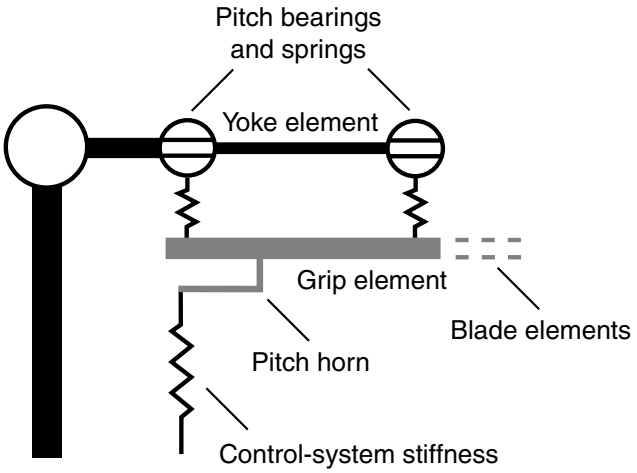

Fig. 9. Schematic of dual load-path model.

For purposes of illustration, Fig. 9 shows the load paths offset vertically. On the actual rotor, the grip is a distorted tube, and its structural axis is coincident with that of the yoke; the CAMRAD II model is set up accordingly. Also, the figure shows only the out-of-plane transverse flexibility, represented as springs.

Both blade models had seven elastic beam elements: a root element, running from the gimbal out to the pitch bearing; a yoke element between the bearings; and five blade elements outboard of the bearings. In addition, the DLP model used one beam element for the grip. The SLP model combined the grip and yoke into one element and deleted the outboard bearing.

In both variants, the control system is modeled with a lumped pitch-link stiffness that includes all rotating and nonrotating elements. (Swashplate coupling is discussed in the next section of this paper.) The two models were individually checked against the Myklestad model (Ref. 12) to match blade frequencies. The SLP flap and lag springs, and the DLP yoke stiffnesses, were adjusted to match the flap and lag frequencies; the pitch link stiffness was adjusted to match the rigid torsion (blade pitch) frequency. (Detailed frequency comparisons are listed in Ref. 10.)

Both blade models had 17 aerodynamic panels. These are more panels than would normally be used for whirl-flutter calculations, but a finer distribution was appropriate for capturing the effects of blade sweep and simulating Ribner's correction (discussed later in this report).

Swashplate coupling

CAMRAD II provides two options for modeling the dynamic coupling between the swashplate and the airframe: the swashplate can be assumed to be fixed with respect to the hub, so that its mode shape is derived from the hub; or its mode shape can be referenced to an arbitrary position, which requires a separate set of mode shape inputs from an external analysis, such as NASTRAN. Both such options are examined here. For the second option, the input mode shapes were referenced to the V-22 transmission adapter, which is the grounding point for the swashplate actuators. For both options, CAMRAD II translates the mode shapes to the trimmed swashplate position, then adds the effects of control system stiffness to the swashplate modal deflections.

Figure 10 illustrates the kinematics of the swashplate motions. In Fig. 10a, the rotor, swashplate and actuators are in their trimmed positions, and the airframe (including the rotor shaft) has no modal deflection. In Fig. 10b, the mode shapes of the hub and transmission are different, so that the hub is deflected with respect to the actuator grounding points. (For clarity, the transmission is shown undeflected.) The parallelogram arrangement of the actuators forces the swashplate to remain parallel to its original, trimmed position, so that there is no change in the cyclic input with respect to the direction of airflow.

In Fig. 10c, the swashplate deflects with the mode shape of the hub, so that there is no change in the cyclic input with respect to the shaft. However, there is now a cyclic input with respect to the direction of airflow. This has a major effect on whirl flutter (Ref. 18). This can occur either because the rotor hub and transmission deflect in unison, or because the actuators themselves extend under dynamic loads, as shown in Fig. 10c.

The swashplate model of Fig. 10c is referred to below as a "uncoupled" swashplate, because it is fixed with respect to the hub, and that of Fig. 10b as a "coupled" swashplate, because its mode shapes are dependent upon the transmission, coupled via the actuators.

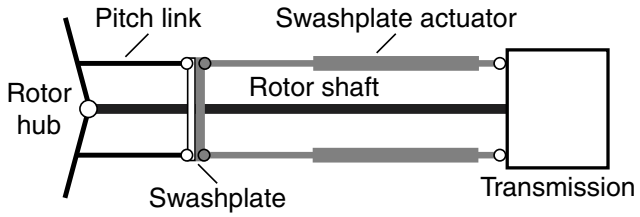

a) Undeflected system.

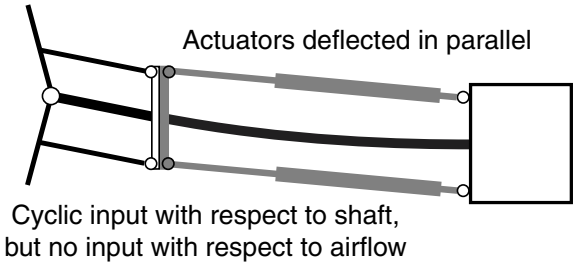

b) Shaft deflected in bending, no transmission deflection or rotation, no actuator extension.

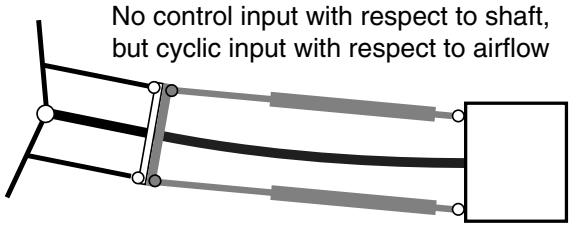

c) Shaft deflected in bending, actuators extended so that swashplate rotates with shaft.

Fig. 10. Kinematic consequences of coupled and uncoupled swashplates.

Figure 11 summarizes the effects on whirl flutter of the different structural models considered so far. The symmetric wing beamwise-bending mode is by far the most strongly affected, so only it is shown. Both the single and dual load-path models are shown with both swashplate modal models. Although two of the curves appear to be very similar, this is believed to be merely coincidental: the dual load-path model and the transmission-coupled swashplate model each add roughly the same amount of damping to the single load-path, rigid-swashplate model. Below about 400 knots, the damping is increased, and above 400 knots, the damping is decreased, so that the variations of damping with airspeed are greatly smoothed out.

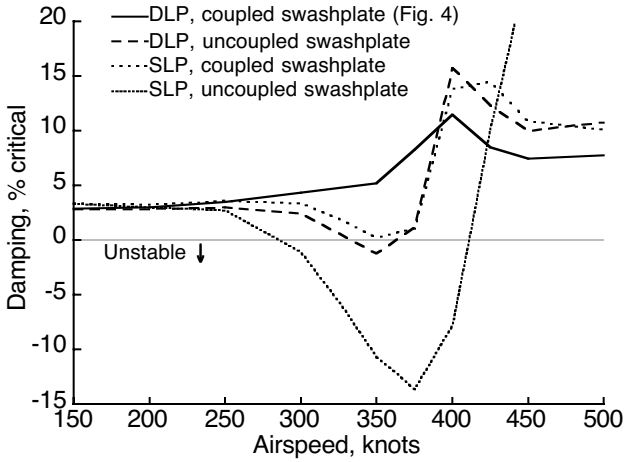

Fig. 11. Predicted symmetric wing beamwise mode damping for different grip and swashplate models.

The reason for the large differences in whirl-mode stability predicted by the single and dual load-path models (with either swashplate model) is explained by the plots of blade mode shapes in Figs. 12-14. The first two figures show in-plane and out-of-plane mode shapes for the first flap and lag modes. (The mode shapes for the SLP model are not calculated inboard of the flap/lag hinge at 0.048 R).

Figure 14 shows the in-plane mode shape for the first lag mode, with the SLP mode shape extended inboard to the radius of the pitch horn attachment to the pitch link. The extended mode shape (the gray line in the figure) follows the slope of the mode shape at the flap/lag hinge. This is equivalent to a rigid pitch horn attached to the blade just outboard of the hinge. The DLP mode shape is much less curved than the SLP shape over the length of the grip, because the DLP shape in this region is determined entirely by the extreme stiffness of the grip.

The kinematics of the couplings between the blade mode shapes and the control system are critical for whirl-mode stability. Figure 14 suggests that the differences in SLP and DLP mode shapes, although not large in an absolute sense, are such as to cause substantially different kinematic couplings at the pitch horn radius. The difference arises from the transverse flexibility of the pitch bearings inside the grip (Figs. 6 and 7), which allows the grip to cock slightly with respect to the yoke, thereby changing the mode shapes near the hub. The effect is less for flap modes than lag modes, because the yoke stiffness is much lower in flapping than lag, which partially relieves flapping moments and reduces the cocking angle.

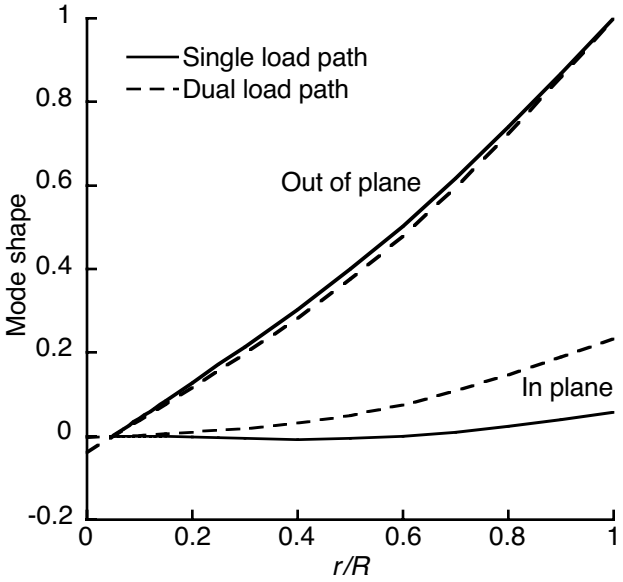

Fig. 12. Mode shapes for the first blade flap mode.

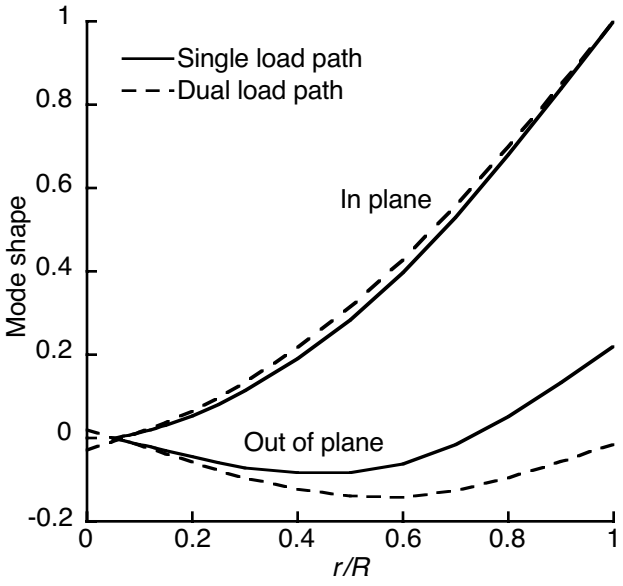

Fig. 13. Mode shapes for the first blade lag mode.

The need to correctly model the kinematic effects of the grip-to-yoke connections through the elastomeric bearings, plus the requirement to fully model the coupling between the swashplate, rotor shaft, and transmission, is not confined to analytical models: construction of a dynamically scaled wind-tunnel model is made extremely challenging by these issues, especially at small scales.

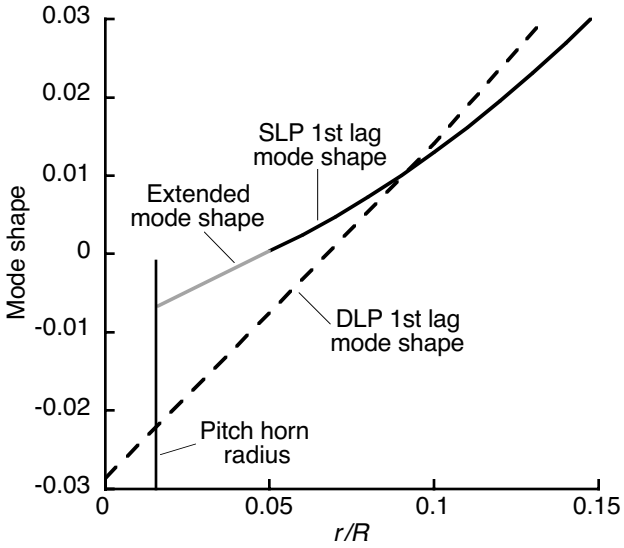

Fig. 14. Mode shapes for the first blade lag mode (expanded scale); extended mode shape is in gray.

Aerodynamic models

CAMRAD II is intended to be used with C81 airfoil tables, but other aerodynamic models are possible. An incompressible flow model is provided in the code. This model uses the nominal zero-Mach values of the C81 tables for all airspeeds. In addition, correction factors can be specified to make CAMRAD II use C81 coefficients at different Mach numbers than those given in the input tables. CAMRAD II can also generate C81 tables from internal equations. These options were used to test the effects of four different compressibility models on the modal predictions. The results are summarized in Fig. 15 for the symmetric wing beamwise mode, which was the most strongly affected mode.

The simplest aerodynamic model is the incompressible case. It yields slightly higher damping predictions at medium airspeeds, and much higher damping at very high speeds. Predicted damping based on the full C81 tables is slightly higher near 400 knots. The difference below 400 knots is reasonable: compressibility should increase the lift curve slope and decrease stability until near the C_{l_α}-divergence speed, when the aft shift in the center of pressure should improve stability compared to the incompressible case.

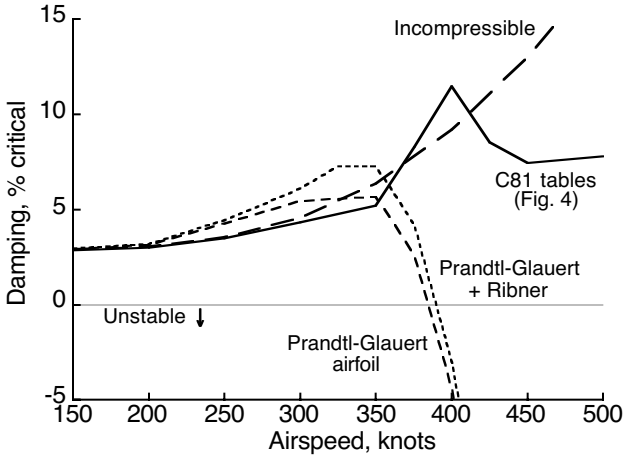

Fig. 15. Predicted symmetric wing beamwise mode damping for different aerodynamic models.

The anomalous behavior above 400 knots appears to be an artifact of the C81 tables, which were generated from wind-tunnel data that were limited in maximum Mach number (Ref. 13). The limiting Mach numbers were different for each airfoil section. For the local Mach numbers at the individual airfoil sections, these limits are all reached at approximately 400 knots forward airspeed. Beyond these limits, the tables contain NACA 0012 airfoil data (modified), hence the C81-table predictions of Fig. 15 are not strictly valid at higher speeds.

Note that scale models, particularly those tested in low-speed, atmospheric-pressure wind tunnels, will operate at lower Mach numbers than the V-22 rotor. For such models, the incompressible model may yield adequate predictions of the damping trends (Ref. 9).

A special airfoil table was generated for the XN-12 airfoil, wherein the lift coefficients were extrapolated from the zero-Mach wind-tunnel data (Ref. 13) using the Prandtl-Glauert correction $1/\sqrt{1-M^2}$. The lift coefficients do not include any C_{l_α}-divergence effects. Stability predictions based on these airfoil data, applied over the entire blade radius, are plotted in Fig. 15. It is obvious that the absence of full compressibility effects drastically lowers the damping at high speeds.

Ribner's correction (Ref. 19) was used in Ref. 12 to further adjust for Mach number effects. Ribner's correction calculates an equivalent Mach number for the rotor as a whole. It can be simulated in CAMRAD II with correction factors chosen to force the C81 table look-ups to occur at the Ribner equivalent Mach number instead of the actual section Mach number. Correction factors were calculated for each aerodynamic panel at every trimmed airspeed, referenced to the local section Mach numbers. The results are plotted in Fig. 15; the main effects of Ribner's correction are to increase damping at medium airspeeds (325 to 375 knots) and to slightly extend the flutter boundary. It should be emphasized that this flutter boundary, at slightly below 400 knots, is based on a simplified aerodynamic model; the actual aircraft may be expected to follow the C81-table predictions.

Bell Helicopter's ASAP analysis (Ref. 12) used the XN-12 airfoil data, extrapolated above zero Mach number by the Prandtl-Glauert correction, which is itself determined by the Ribner equivalent Mach number. Hence, the "Ribner" predictions of Fig. 15 approximate the methods used to verify the V-22 whirl-flutter margins against design specifications, as detailed in Ref. 12. Reference 10 shows CAMRAD II predictions for all whirl modes; they are generally similar to those generated by ASAP. The most significant overall differences are that CAMRAD II predicts much larger variations in damping over the airspeed range, and for some modes predicts larger changes in frequency with airspeed, although the general patterns are the same.

Drive train models

The effects of the drive-train model are illustrated in Figs. 16 and 17; only the most strongly affected modes are shown. In Fig. 16, the alternative model has a simple "rigid" drive train, wherein all rotating masses are coupled to the rotors, but there are no internal dynamics. In Fig. 17, the alternative model has no drive train at all.

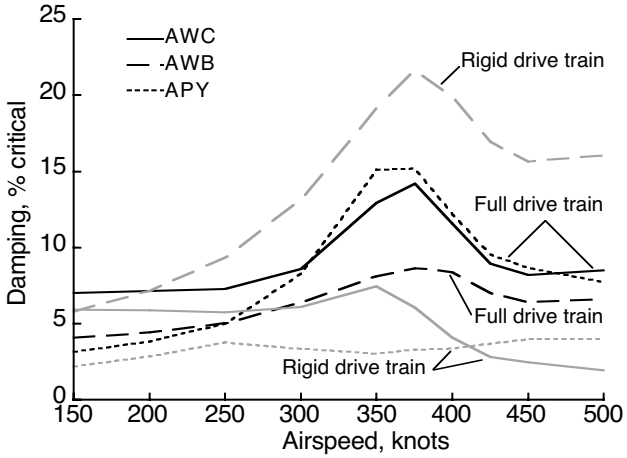

Fig. 16. Predicted damping of the V-22 antisymmetric wing/pylon modes, with flexible and rigid drive train models. Predictions for the rigid model are in gray.

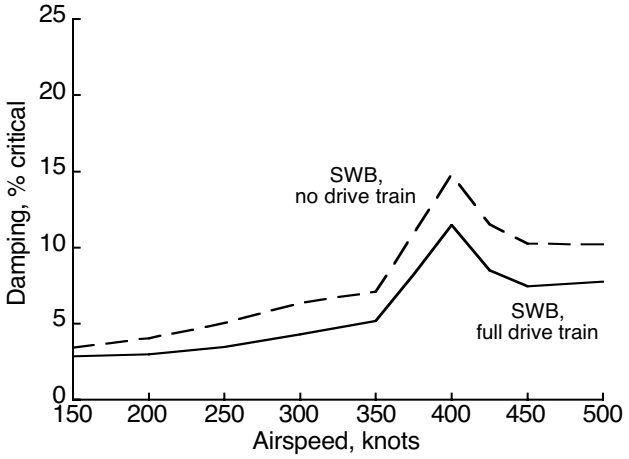

Fig. 17. Predicted damping of the V-22 symmetric wing beamwise mode, with and without a drive train model.

The results are generally as expected: eliminating drive-train flexibility (the rigid drive train model) affects only the antisymmetric modes; eliminating the drive train entirely further affects only symmetric modes (and only one of them). The wing beamwise-bending modes, symmetric and antisymmetric (SWB and AWB) are the most strongly affected, both exhibiting a significant loss of damping when the drive train is included.

The need to model these drive-train effects must be taken into account during the design and testing of dynamically scaled wind-tunnel models.

EFFECTS OF ROTOR DESIGN VARIATIONS

Delta-3 Effects

Because it is already stable, the baseline model (Figs. 2-5) is not convenient for analyzing the effects of rotor design on aeroelastic stability. However, it is a simple matter to destabilize the rotor by changing the pitch/flap coupling (δ_3). As defined herein, positive δ_3 causes nose-down pitching for upwards blade flapping (Fig. 18). For the present study, δ_3 was always changed by adjusting the distance of the pitch horn from the flapping axis. Such a modification does not affect the structure or aerodynamics of the individual blades, so its effects on aeroelastic stability are not confounded with those of the other design changes considered below.

The values of δ_3 given here are nominal, at-rest values with the pitch horn level. The coning flexure reduces the effective kinematic value, as does any control input that rotates the pitch horn away from the level position.

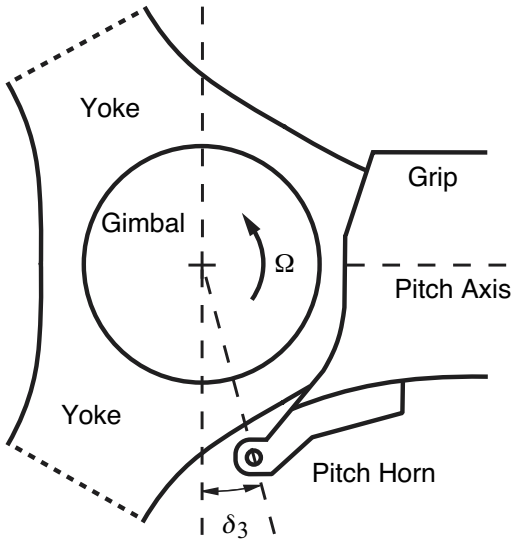

Fig. 18. Kinematics of V-22 hub and pitch horn, showing design δ_3 of –15 deg.

Figures 19 and 20 show the effects on whirl modes of changing δ_3; only adversely affected modes are shown. It was shown in Ref. 20 that negative δ_3 is required for proprotor stability, so only negative values of δ_3 were examined here. A reference airspeed of 300 knots was chosen to keep the rotor within its design envelope, but near the upper limit.

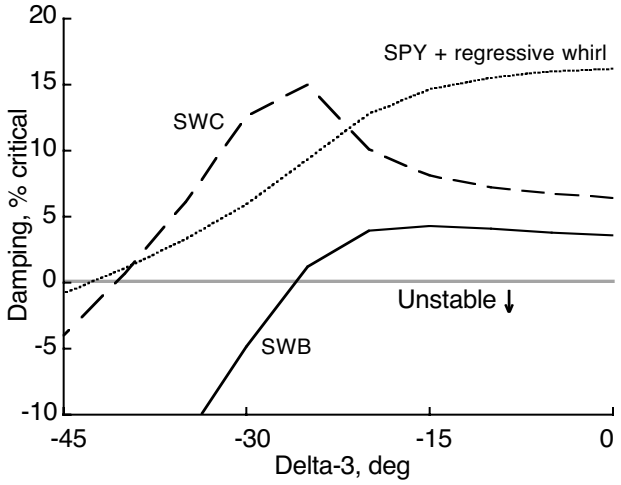

Fig. 19. Variation of damping with δ_3 for the unmodified V-22 rotor at 300 knots. Only adversely affected symmetric modes are shown.

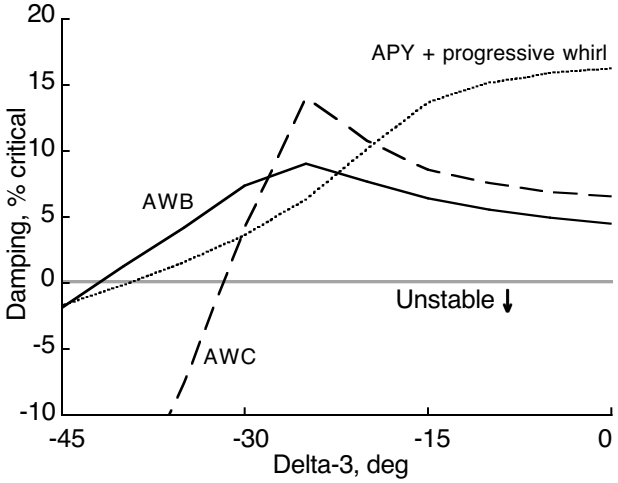

Fig. 20. Variation of damping with δ_3 for the unmodified V-22 rotor at 300 knots. Only adversely affected antisymmetric modes are shown.

The trend in stability follows the classic pattern: the rotor remains stable until δ_3 approaches –20 deg, then the least stable mode (in this case, the SWB mode) rapidly loses stability as the magnitude of δ_3 becomes more negative. The torsion and pylon yaw modes remain stable and are not shown. However, two highly coupled modes, both involving primarily pylon yaw and cyclic rotor whirl modes, do become slightly unstable at very high values of δ_3.

The values shown here are for a level pitch horn; the actual value varies slightly with blade pitch. The design value of δ_3 for the V-22 is –15 deg, which provides an adequate stability margin. A value of –30 deg was chosen for the design studies discussed below. The challenge is to stabilize the SWB mode, and if possible increase the stability margin for the AWC mode, without degrading the other modes. Even larger values of δ_3 are desirable for advanced rotor designs, in particular those with more than three blades.

Blade Sweep and Tip Mass Offset

To stabilize the rotor with –30 deg δ_3, combinations of blade sweep and tip mass offset were studied. Figure 21 shows an example swept blade derived from the V-22 rotor. For this rotor, the primary significance of sweep is the improved whirl-flutter boundary, not the reduced Mach-number effects. An offset tip mass is also shown; it is simply the existing balance weight offset from its normal position. (The balance weight is located slightly inboard of the tip, as shown.)

For this CAMRAD II model, blade sweep was invoked by sweeping the elastic axis and airfoil quarter-chord line by a sweep angle Λ, positive aft, starting at a radial station r_s. For these initial studies, r_s was always 80% R. The tip mass was offset from its design location a distance x_m, positive forward. The entire mass was always moved. Sweep was always calculated in the local chord plane, so it followed the blade twist. Tip mass offsets were also always in the local chord plane. The maximum sweep analyzed is equivalent to less than one chord length at the tip.

Tip mass offset x_m is presented here in terms of equivalent sweep Λ, where

$$\Lambda = \sin^{-1}\left(\frac{x_m}{R - r_s}\right).$$

For blade sweep only (Fig. 22), the tip mass was offset aft of the pitch axis with the rest of the blade so that it maintained the same position with respect to the elastic axis. For tip mass offsets only (Fig. 23), the tip mass was offset forward of the pitch axis.

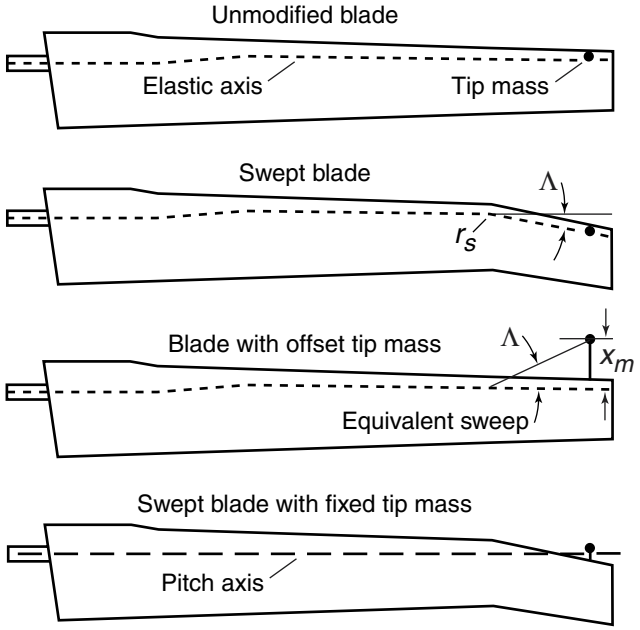

Fig. 21. V-22 rotor blade planform (47.5-deg nonlinear twist not shown).

Figures 22 and 23 show the effects of sweep and tip mass offsets on damping. The magnitudes of blade sweep and tip mass equivalent sweep are the same, but the signs are reversed. Most modes were little affected and are not shown. The most responsive modes — SWB and AWC — were the least stable, which is encouraging. The SWT mode damping decreased slightly with sweep (Fig. 22) but was little affected by tip mass offsets (Fig. 23). Note that the effects of sweep on damping are nonlinear, unlike the effects of tip mass offset. Sweep values beyond 30 deg were not examined

because the SWB and SWT damping curves intersect (Fig. 22), after which sweep reduces stability.

Figure 24 illustrates the effects of combining sweep and tip mass offset, with the forward tip mass offset of Fig. 23 added to the aft blade sweep of Fig. 22. Sweep and mass offset were incremented by the same magnitudes but with opposite signs. The effects are highly nonlinear, with the SWB mode damping increasing very rapidly at the maximum value of sweep examined. Damping of the AWC mode reaches its maximum value at about 25 deg of sweep, but it is so stable that the limit is of no practical consequence. Large values of sweep combined with large mass offsets are not practical anyway, because of the very long mass support required.

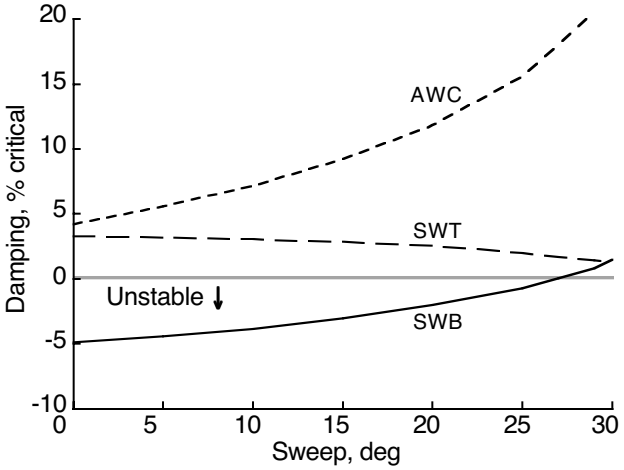

Fig. 22. Variation of damping with blade sweep at 300 knots with –30 deg δ_3.

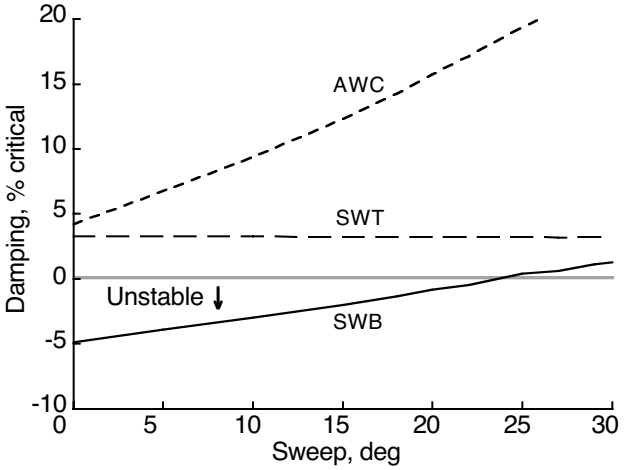

Fig. 23. Variation of damping with tip mass offset at 300 knots with –30 deg δ_3. Offset is calculated as equivalent sweep.

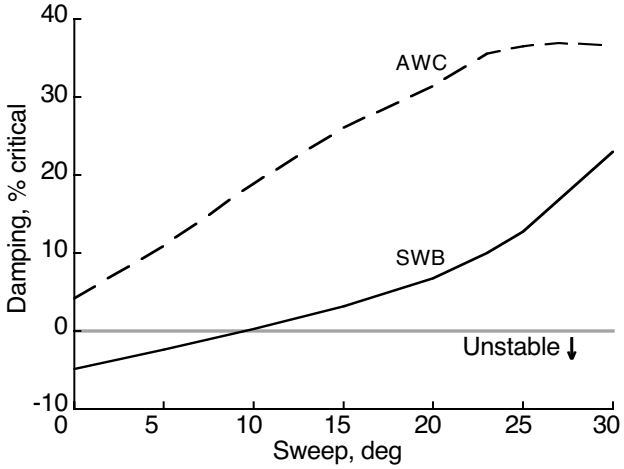

Fig. 24. Variation of damping with combined sweep and tip mass offset at 300 knots with –30 deg δ_3. Offset is calculated as equivalent sweep.

Figure 25 shows the effects of sweep with the tip mass fixed at its original position with respect to the blade pitch axis, which is perhaps a more practical configuration. The SWT mode damping decreases very slightly with sweep, so that the optimum value of sweep is about 22 deg.

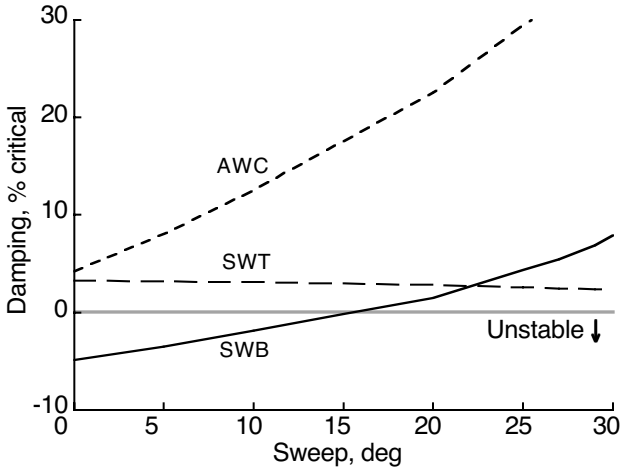

Fig. 25. Variation of damping with sweep and fixed tip mass position at 300 knots with –30 deg δ_3. Offset is calculated as equivalent sweep.

For ease of comparison, the predictions for SWB mode damping are replotted in Fig. 26. The figure emphasizes the effects of mass offset on both the sensitivity of damping to sweep, and on the nonlinearity of the responses. An offset tip mass would have to be placed on a boom extending from the leading edge, or within a large fairing. The benefit to damping makes such a unorthodox design worth considering in addition to blade sweep.

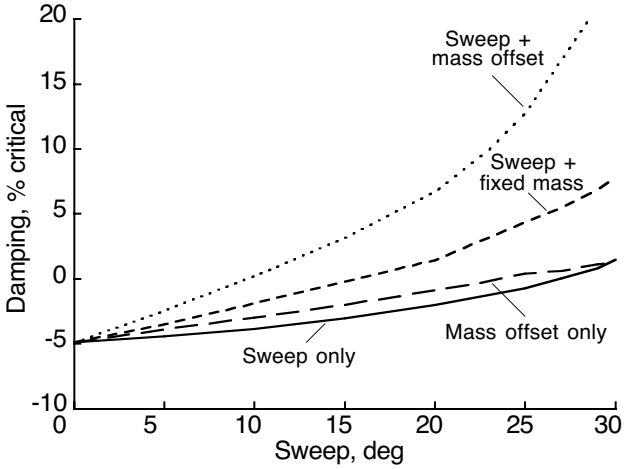

Fig. 26. Comparison of the effects of sweep and mass offset on the SWB mode at 300 knots with –30 deg δ_3. Offset is calculated as equivalent sweep.

An initial survey of pitch-link loads was made to check for potentially serious changes. Mean pitch-link loads were calculated for each configuration of blade sweep and mass offset examined. The elastomeric-bearing torques were subtracted to emphasize the differences due to blade design changes, then the residual pitch link loads were scaled to those for the baseline rotor (zero sweep and mass offset) at –30 deg δ_3 (Fig. 27). Because the rotor was trimmed in axisymmetric flow, only the mean loads were examined, based on the trimmed blade deflections.

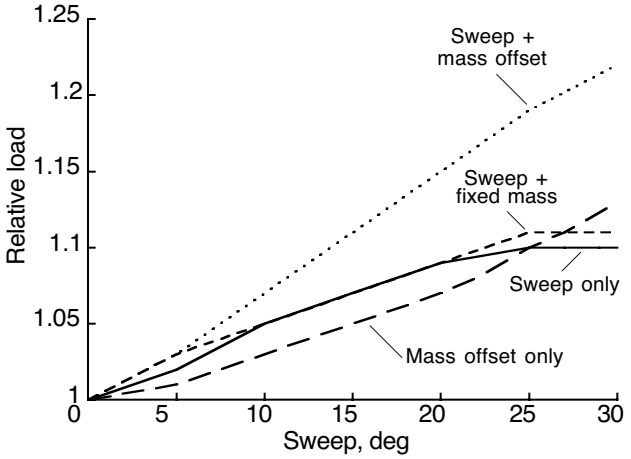

Fig. 27. Pitch-link load increase as a function of blade sweep and tip mass offset, calculated at 300 knots with –30 deg δ_3.

The largest load increase was 22%, for the combined sweep and tip mass offset. Although not trivial, this increase is not excessive, especially considering that no attempt was made to retune the blade for lower loads. While admittedly only a cursory survey, these results are encouraging. A more comprehensive loads survey would be required as part of any further design efforts.

MODEL IMPROVEMENTS

There are several possible areas of improvement for the CAMRAD II model of the V-22 rotor, discussed here in three groups: control system kinematics, grip/yoke model, and aerodynamics. Some of the deficiencies have been discussed previously and are summarized here for convenience.

(As of this writing, CAMRAD II Release 4.1 will shortly be available. It will offer new options that should facilitate some of the proposed improvements, particularly the grip/yoke model and the wake model.)

Control system kinematics

An improved control-system stiffness model could be constructed with separate inputs for pitch-link, pitch-bearing, and swashplate flexibility (collective and cyclic), including displacement offsets and preloads. Because of the good matches to Myklestad blade frequencies and to the ASAP whirl-flutter predictions, no refinements to the current CAMRAD II lumped-stiffness model were made. However, a more sophisticated model would be needed to properly calculate loads.

The coupled swashplate model (Fig. 10b) is not exact: applying the mode shapes of the transmission adapter to the swashplate is only an approximation to the actual kinematics. A better approach would be to explicitly model the nonrotating actuators. Although the kinematic differences are expected to be small, the high sensitivity of whirl-mode damping to control-system kinematics suggests that such an improved model is worth pursuing.

Grip/yoke model

The CAMRAD II structural model follows the general pattern of the Myklestad segmented model in Ref. 12, which distributes inertias evenly within each segment. In some cases, such as the pitch horn, the radial position of a significant mass is known more accurately than the Myklestad data alone. The CAMRAD II model could be improved to more accurately locate the radial centers of gravity of each segment. The current mass distribution gave

good results, so an improved model was unnecessary for the present research.

The single load-path model could be improved by shifting the flap and lag hinges outboard to the effective centers of rotation of the first flap and lag modes. However, close attention must be paid to the order of the hinges — flap, lag, pitch — with any significant masses connected to the correct side of each hinge. Given the good results with the dual load-path model, there was little incentive to further refine the single load-path model. However, such a model would be appropriate for design of dynamically scaled models, for which duplication of the dual load-path grip and yoke may be impractical.

Aerodynamics

The C81 tables are a major limitation for stability analyses. The area of concern is limited to very high speeds, so the effects on the present research are thought to be negligible. However, establishment of reliable stability trends at high speeds is still desirable and could benefit from improved aerodynamic tables. Repeating the wind-tunnel airfoil tests at higher Mach numbers would be expensive, but modern CFD methods should be able to produce completely adequate data. The key requirement is to generate coefficient data at Mach number increments small enough to guarantee that all significant variations are captured near C_{l_α}-divergence, and to eliminate the possibility of numerical artifacts arising from interpolation from nonlinear data.

Very little attention was paid to airframe aerodynamics during this research. It is largely irrelevant for power-off stability, and the wing-body aerodynamic tables are adequate for power-on stability analyses. Obvious avenues for future improvements are to generate a comprehensive set of CAMRAD II wing-body tables for all nacelle angles, or possibly to update the coefficients used by the internal aerodynamic model.

SIMPLIFIED MODELS

The improvements suggested above all make the CAMRAD II model more complicated, with the undesirable side effects of making parametric variations more cumbersome and the interpretation of analytical results more difficult. Simpler models would help to clarify the mechanisms by which sweep works, which are necessary to efficiently guide design optimization studies. (The nonlinearities shown in Figs. 22, 24, 25 and 26 cannot be explained by the "classical" whirl-flutter analyses of, for example, Refs. 6 and 21.)

An obvious approach to a simplified model is to linearize the blade property distributions, at least over the swept region, and to approximate the grip/yoke assembly with a single load-path model, as previously suggested. Although such a model would not predict stability well at high speeds, it would be an adequate approximation within the V-22 design envelope.

As a first step towards a better understanding of the effects of sweep and mass offset, studies were initiated to determine the minimum number of modes needed to capture the general trends of stability with airspeed and to duplicate the nonlinear effects of sweep.

The baseline dynamic model, with eight dynamic and 16 quasi-static modes per blade, was possibly over-modeled. The damping trends with airspeed were closely approximated with only four dynamic and five quasi-static modes per blade, as shown in Figs. 28 and 29; compare with Figs. 4 and 5. The dynamic modes extended to 6/rev and included the first flap, lag and torsion modes, plus the second flap mode; the quasi-static modes extended to 16/rev. While there are numerous differences in detail, the overall trends with airspeed are very similar up to 450 knots, well beyond the flight envelope. (The differences became severe thereafter, so the plot was truncated to avoid distorting the vertical scale.)

In contrast, the minimum number of blade modes needed to capture the nonlinear effects of blade sweep and mass offset were two dynamic (first flap and lag) and ten quasi-static modes (through 30/rev). Eliminating the drive-train modes shifted the zero-sweep and zero-offset baselines, but did not change the trends. The results are shown in Figs. 30 and 31; compare with Figs. 22 and 23.

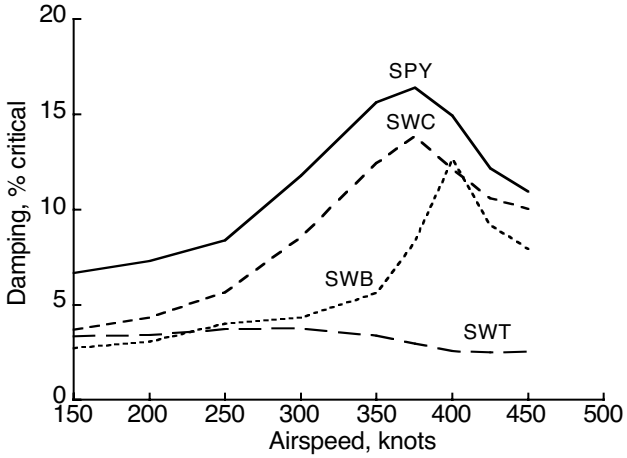

Fig. 28. Symmetric wing/pylon mode damping predicted by the simplified model (nine blade modes).

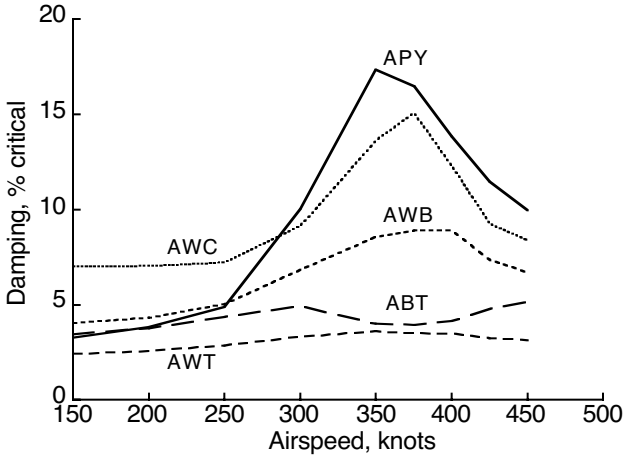

Fig. 29. Antisymmetric wing/pylon mode damping predicted by the simplified model (nine blade modes).

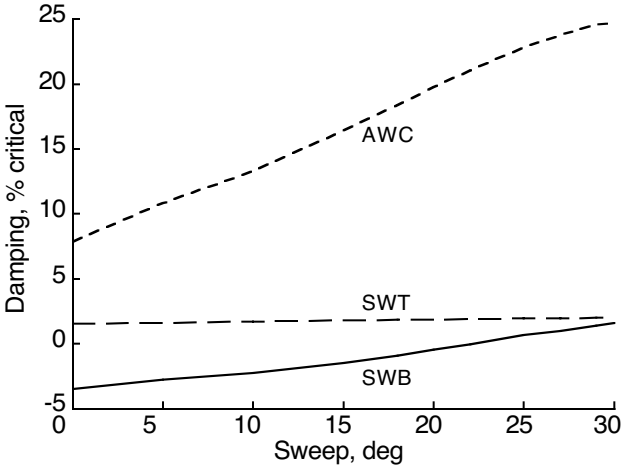

Fig. 31. Variation of damping with tip mass offset at 300 knots with –30 deg δ_3, using the simplified model (twelve blade modes and no drive train).

The large number of blade modes needed is disturbing, because it threatens to frustrate, or at least excessively complicate, attempts to fully understand the mechanisms by which blade sweep and mass offsets affect damping. Significant progress requires distinguishing between several possible physical effects of sweep and mass offset. A swept tip has a larger moment arm about the pitch axis for both aerodynamic and inertial forces. A swept airfoil has a lower effective Mach number and a reduced C_{l_α}. Mass offsets change both the moment arm and the magnitude of the inertial forces, the latter because of the change in distance from the hub plane (effective droop; see Ref. 21). There are also changes in blade mode shapes and frequencies, which depend strongly on the details of the dual load-path hub (Fig. 14).

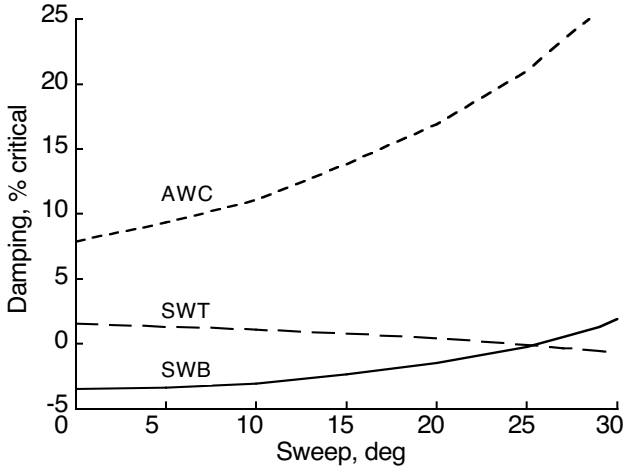

Fig. 30. Variation of damping with blade sweep at 300 knots with –30 deg δ_3, using the simplified model (twelve blade modes and no drive train).

These issues are a ripe area for further research, which will probably require simplified V-22 models to separate the effects of the dual-load path hub, kinematics of pitch-lag coupling, and blade structural characteristics.

RECOMMENDATIONS

Useful areas of improvement to the CAMRAD II model of the V-22 have already been discussed. It is of at least equal importance to acquire experimental data to support the analytical results presented here. Of the V-22 design features that have been shown to have important effects on whirl-mode stability, several will be difficult to duplicate at small scale. These include the drive train, swashplate coupling, and the elastomeric bearings between the grip and yoke.

The Wing and Rotor Aeroelastic Testing System (WRATS; Ref. 22) is the best dynamically-scaled model of the V-22 in use today, and it does not duplicate all of these effects. As a prelude to any experimental testing of sweep or mass offsets, a thorough CAMRAD II analysis of the as-built rotor system installed on the WRATS should be carried out. WRATS has been thoroughly analyzed throughout its history (Ref. 22), but not for the types of rotor modifications proposed here.

The overall effects of sweep and mass offset do not depend upon the details of the V-22 rotor: broadly similar results are predicted for the much-simpler XV-15 rotor system (Ref. 8). It should be possible to demonstrate the effects with a simpler rotor, and possibly with a simpler test stand, than the WRATS. In any event, it would be an instructive exercise to analytically determine the simplest rotor system for which sweep and mass offsets make a significant improvement to

whirl-mode stability. This would provide a better understanding of the mechanisms by which sweep and mass offsets alter aeroelastic stability. Such an effort is currently underway at NASA Ames Research Center.

The research would naturally lead to design optimization studies, once the interactions between possible design modifications are fully understood. The designs studied here were arbitrarily limited to constant sweep over a constant radius. Proper optimization should obviously consider different sweep angles over different radial extents, plus curved tips with varying sweep angles. Also, sweep need not be in the local chord plane, but could be skewed at different angles to the rotor plane.

Mass offsets could vary in total mass, distance from the leading edge, and distance from the tip. Earlier work (Ref. 9) suggests that a chord-balance mass placed at the radius of sweep onset could be effective. This would be more aerodynamically and structurally practical, as pointed out by David A. Popelka of Bell Helicopter. A similar concept can be found in Ref. 23.

CONCLUSIONS

The V-22 was analyzed with CAMRAD II to evaluate whirl flutter in airplane-mode flight. The stability predictions were sensitive to the details of the grip/yoke model: a dual load-path model was necessary to properly predict damping. Coupling of the swashplate modes to the transmission, instead of to the rotor hub, also had a large effect on damping. The drive-train model proved important, as expected. Use of C81 tables, derived from wind-tunnel data, for rotor aerodynamics gave much different predictions than an aerodynamic model based on a Prandtl-Glauert lift-curve slope and Ribner's correction.

The effects of blade sweep and tip mass offsets on whirl-flutter stability were examined. The rotor was (analytically) destabilized by increasing the magnitude of pitch-flap coupling to –30 deg. The outer 20% of the blade was swept aft a maximum of 30 deg (about one chord length) and the tip balance weight was offset forwards by the same amount. Different combinations of blade sweep and mass offset were evaluated; the most favorable combinations greatly increased the damping of the least stable modes, more than enough to fully stabilize the rotor. A simple survey of pitch-link loads indicated an increase of 22% for the worst case.

This research has touched merely a small part of the range of possible rotor modifications that could improve whirl-flutter margins. Efforts are proceeding towards a deeper analysis of the effects of sweep on stability, with a longer-term goal of wind-tunnel tests of the concept.

ACKNOWLEDGEMENTS

The author wishes to thank Wayne Johnson for his unfailing support and encouragement for this research, and David A. Popelka for his generous assistance in providing data and advice for modeling the V-22.

REFERENCES

1. Corrigan, J. J., Bennett, R. L., Hsieh, P. Y., "COPTER 2000: The QTR and Beyond," American Helicopter Society 57th Annual Forum, Washington, DC, May 2001.

2. Nixon, M. W., Piatak, D. J., Corso, L. M., Popelka, D. A., "Aeroelastic Tailoring for Stability Augmentation and Performance Enhancements of Tiltrotor Aircraft," American Helicopter Society 55th Annual Forum, Montréal, Quebec, Canada, May 1999.

3. Kvaternik, R. G., Piatak, D. J., Nixon, M. W., Langston, C. W., Singleton, J. D., Bennett, R. L., and Brown, R. K., "An Experimental Evaluation of Generalized Predictive Control for Tiltrotor Aeroelastic Stability Augmentation in Airplane Mode of Flight," American Helicopter Society 57th Annual Forum, Washington, DC, May 2001.

4. Matuska, D., Sacullo, A., and Studebaker, K., "Reduced Tip Speed Testing of a Variable Diameter Tiltrotor, " 19th European Rotorcraft Forum, Cernobbio (Como), Italy, September 1993.

5. Madden, J. F. III, and Peyran, R. J., "Aeroelastic Stability Enhancer for Tilt-Rotor Aircraft," Invention Disclosure, NASA Case No. ARC-14298-1CU, May 1998.

6. Srinivas, V., Chopra, I., and Nixon, M. W., "Aeroelastic Analysis of Advanced Geometry Tiltrotor Aircraft," *Journal of the American Helicopter Society*, Vol. 43, No. 3, July 1998.

7. Dadone, L., Liu, J., Wilkerson, J., and Acree, C. W., "Proprotor Design Issues for High Speed Tiltrotors," American Helicopter Society 50th Annual Forum, Washington, D.C., May 1994.

8. Acree, C. W., Peyran, R. J., and Johnson, W., "Rotor Design Options for Improving Tiltrotor Whirl-Flutter Stability Margins," *Journal of the American Helicopter Society*, Vol. 46, No. 2, April 2001.

9. Acree, C. W., "Effects Of Rotor Design Variations On Tiltrotor Whirl-Mode Stability," Tiltrotor/Runway Independent Aircraft Technology and Applications Specialists' Meeting, Arlington, TX, March 2001.

10. Acree, C. W., "A CAMRAD II Model of the V-22 Rotor for Whirl-Flutter Analysis," NASA TM (in preparation).

11. Johnson, W., "CAMRAD II Comprehensive Analytical Model of Rotorcraft Aerodynamics and Dynamics — Theory Manual," Johnson Aeronautics, Palo Alto, CA, 1993.

12. Parham, T. and Froebel, A., "V-22 EMD Intermediate Flutter and Divergence Report," Bell-Boeing Report no. 901-910-039, September 1997.

13. Jenks, M. D. and Narramore, J. C., "Final Report for the 2-D Test of Model 901 Rotor and Wing Airfoils (BSWT 592)," Bell-Boeing Report No. D901-99065-1, May 1984.

14. Brunken, J. E. and Vlaminck, R. R., "V-22 MSC/NASTRAN Airframe Vibration Analysis and Correlation," National Technical Specialists' Meeting on Rotorcraft Dynamics, Arlington, TX, November 1989.

15. Idol, R., and Parham, T., "V-22 Aeroelastic Stability Analysis and Correlation with Test Data," American Helicopter Society 51st Annual Forum, Ft. Worth, TX, May 1995.

16. Thrasher, L., "V-22 Main Rotor Yoke Thickness," American Helicopter Society 57th Annual Forum, Washington, D.C., May 2001.

17. Popelka, D., Sheffler, M., and Bilger, J., "Correlation of Test and Analysis for the 1/5-Scale V-22 Aeroelastic Model," *Journal of the American Helicopter Society*, Vol. 32, No. 2, April 1987.

18. Hall, W. E., Jr., "Prop-Rotor Stability at High Advance Ratios," *Journal of the American Helicopter Society*, Vol. 11, No. 2, April 1966.

19. Ribner, H. S., "Propellers in Yaw," NACA Report No. 820, 1945.

20. Gaffey, T. M., "The Effect of Positive Pitch-Flap Coupling (Negative δ_3) on Rotor Blade Motion Stability and Flapping," *Journal of the American Helicopter Society*, Vol. 14, No. 2, April 1969.

21. Johnson, W., "Analytical Modeling Requirements for Tilting Proprotor Aircraft Dynamics," NASA TN D-8013, July 1975.

22. Piatak, D. J., Kvaternik, R. G., Nixon, M. W., Langston, C. W., Singleton, J. D., Bennett, R. L., and Brown, R. K., "A Wind-Tunnel Parametric Investigation of Tiltrotor Whirl-Flutter Stability Boundaries," American Helicopter Society 57th Annual Forum, Washington, D. C., May 2001.

23. Dadone, L., Derham, R., Liu, L., Wilkerson, J., Yablonski, M, and Ziegenbein, P., "Detailed Rotor Design Trade Study," Final Report, NASA Contract NAS2-13607, August 1993.